Ultra-thin film solid oxide fuel cells utilizing un-doped nanostructured zirconia electrolytes

Changhyun Ko*, Kian Kerman, Shriram Ramanathan

Harvard School of Engineering and Applied Sciences, Harvard University, Cambridge, MA 02138, USA

ABSTRACT

Aliovalently-doped zirconia (ZrO_2) systems such as yttria-stabilized ZrO_2 (YSZ) have been explored as ionic conductors for solid oxide fuel cells (SOFCs) owing to their high ionic conductivity and exceptional mechanical and chemical stability. Thin film micro-SOFCs (μ-SOFCs) with free-standing membranes create an opportunity for reduced temperature operation with the need to engineer the various materials components. In this study, we have fabricated μ-SOFCs composed of nominally pure ZrO_2 electrolytes (down to sub-10 nm thickness) prepared by room temperature photon-assisted oxidation of Zr precursor metal films and nanoporous Pt electrodes and report on fuel cell performance up to ∼500 °C in hydrogen. The μ-SOFCs exhibit maximum power density of ∼33 mW cm^{-2} with open circuit voltage of ∼0.91 V at 450 °C. The electrolyte thickness-dependent functional properties of the μ-SOFCs are discussed in detail along with thermo-mechanical stability and microstructural studies. The results could serve as a benchmark to understand doping effects in designing thin film fast-ion conducting zirconia-based electrolytes for low temperature fuel cell operation.

© 2012 Elsevier B.V. All rights reserved.

1. Introduction

Solid oxide fuel cells (SOFCs) have several potential desirable attributes including high energy conversion efficiency and fuel flexibility [1–3]. Reduction in their operating temperature from typical values of ∼800 °C down to 300–500 °C could enhance the scope of their applications into the mobile energy space [4]. Utilizing ultra-thin film electrolytes in the sub-100 nm range enables a reduction in Ohmic resistance and is one approach to realizing low temperature SOFCs [5,6]. This miniaturized SOFC based on thin film structure is called micro-SOFC (μ-SOFC). Much research is needed in synthesis of thin film nanostructured oxides with controlled microstructural defects and their role in device characteristics. Similarly, interpretation of electrical properties of such ultra-thin layers is a formidable problem and is worthy of research itself.

Cation-doped zirconia such as yttria-stabilized zirconia (YSZ) has been incorporated into the majority of SOFCs as an electrolyte due to high ionic conductivity arising from oxygen vacancies as well as excellent mechanical and chemical stability. ZrO_2 has three different structural polymorphs namely cubic fluorite, tetragonal, and monoclinic structures. The high temperature cubic phase is stabilized by aliovalent acceptor doping such as Ca, Mg, Sc, and Y. For each dopant, the doping concentration range for stabilizing the cubic phase varies and is temperature-dependent (for example, the optimal Y_2O_3 doping level for stabilizing cubic phase in bulk ceramic form is 8–9 mol%) [7,8]. Particularly for μ-SOFCs, YSZ thin films are synthesized at lower temperatures (<600 °C) limiting the size of grains to nanoscale range. How such nanostructuring influences electrical conduction in oxides is an interesting area of study and further their impact on fuel cell performance is of importance. Recently, Jung et al. observed that nanocrystalline film shows higher ionic conductivity than bulk counterparts and its peak conductivity is achieved at much lower Y doping level in comparison to bulk YSZ ceramics. They argued that it is due to the formation of metastable cubic phase with smallest defect interaction leading to the largest ionic mobility among the ZrO_2 phases [9]. Brossmann et al. found that grain boundary oxygen-ion diffusion is faster than bulk diffusion by 3–4 orders in magnitude in monoclinic un-doped ZrO_2 ceramics with 70–300 nm grain size by tracer diffusion and secondary ion mass spectroscopy [10]. Eder and Kramer extracted both electronic and ionic conductivities of nanocrystalline monoclinic ZrO_2 bulk samples treated under oxidizing and reducing environments by impedance spectroscopy techniques [11]. The authors observed that the conductivity is increased in the reduced samples likely due to the formation of oxygen vacancies. The μ-SOFC structure is a model system to study this problem in an application context in the intermediate

temperature range (400–600 °C): functional characteristics such as open circuit voltage (OCV) and power density are influenced by oxygen transport in electrolyte [2,3,12]. Perhaps in a broader context, if one could realize high performance fuel cells at these reduced operating temperatures with minimal use of rare earth components, their cost could be lowered. The goal of this study is to understand the performance of un-doped zirconia as an electrolyte in ultra-thin film SOFCs. This may allow a critical comparison of present efforts to realize low temperature fuel cells with improved electrolytes and whether improving ionic conductivity of electrolytes leads to performance gain in such temperature regimes in these device architectures.

In this study, we demonstrate μ-SOFCs based on self-supported nanostructured un-doped ZrO_2 thin films (∼8–70 nm thickness) along with detailed investigation on the thickness-dependent functional properties. In addition, the conduction in un-doped ZrO_2 membranes was evaluated using electrochemical impedance spectroscopy (EIS) technique. Pure ZrO_2 electrolytes were grown by ultra-violet (UV) oxidation from precursor Zr metal films at room temperature (RT). UV illumination creates highly reactive oxygen radicals and ozone molecules and hence, can be employed for synthesizing dense and high-quality ultra-thin oxide films [13,14]. The relatively low oxidation temperature makes this technique desirable for avoiding degradation during fabrication processes. We have also investigated the structural characteristics of ZrO_2 thin films using X-ray diffraction (XRD).

2. Experimental

2.1. ZrO_2 film synthesis and characterization

ZrO_2 films were grown by Zr metal deposition by sputtering and subsequent *in-situ* UV oxidation in a custom-designed load-lock chamber. First, Zr film is grown up to ∼4 nm at d.c.-sputtering gun power of 100 W at RT. The chamber pressure was kept at 5 mTorr with Ar gas during deposition. Then, the samples were transferred to the load-lock chamber and the precursor metal films were oxidized under UV irradiation flowing O_2 gas at 1 atm and RT for 15 min. The UV source is a set of halogen lamps emitting radiation whose primary wave lengths are 254 nm and 185 nm that enables dissociation of the oxygen molecules to form atomic oxygen. The fully oxidized film is self-limiting to ∼5 nm thickness [14,15]. The load-lock chamber was pumped down to high vacuum after UV oxidation and the aforementioned steps were repeated to obtain various thickness ZrO_2 films. The as-grown films were further oxidized under UV irradiation for additional 1 h to improve crystalline quality. Glancing incidence XRD (incidence angle $\Omega = 1°$) was performed for structural analysis of ZrO_2 films grown on Si substrates coated with Si_3N_4 layers on Bruker AXS D8 XRD system with Cu Kα source. The electrolyte film thickness was measured by X-ray reflectivity on Scintag XDS 2000 X-ray diffractometer using Cu Kα source.

2.2. Fuel cell device fabrication and measurements with Pt electrodes

Thin film ZrO_2 electrolyte-based μ-SOFC structures were fabricated on silicon nitride (Si_3N_4)-coated Si employing photolithography, reactive ion etching (RIE), and anisotropic etching using KOH solution. For electrodes, porous Pt layers were used owing to their good catalytic properties. The detailed μ-SOFC device fabrication is as follows: (1) one side of Si wafers sandwiched with Si_3N_4 coatings is patterned by photolithography and the uncoated regions of Si_3N_4 with photoresist are removed by RIE with the process gas mixture of O_2 and CH_4. (2) Si is selectively etched using 30 wt.% KOH

solution at 70–80 °C forming free-standing Si_3N_4 membranes. (3) ZrO_2 electrolyte films are grown on non-etched side of Si_3N_4 membranes (cathode side). In this work, the thickness of ZrO_2 films is varied in the range from ∼8 nm to ∼108 nm (4) ∼55 nm-thick porous Pt cathode thin layer is deposited on electrolyte/Si_3N_4 layers by d.c.-sputtering technique in 75 mTorr Ar pressure at RT and 100 W gun power. (5) After removing Si_3N_4 from the etched window side (anode side) by RIE, porous Pt anode is grown up to ∼40 nm on the anode side at RT with d.c. gun power of 100 W maintaining Ar pressured at 85 mTorr, finally producing Pt/ZrO_2/Pt μ-SOFC structures. The thickness of Pt electrodes was estimated by cross-sectional scanning electron microscopy (SEM) using Carl Zeiss Ultra 55 field emission scanning electron microscope (FESEM). Each chip has a dimension of 10 mm × 10 mm × 0.5 mm containing nine square-shape membranes of 160×160 μm² size. To examine the effects of annealing on the fuel cell functionality, thermal annealing was carried out on ZrO_2 membranes of chosen thicknesses in reducing and oxidizing environments created by 3% H_2/N_2 and 100% O_2 gas respectively for 30 min at 600 °C.

Fuel cell experiments were performed in a home-built fuel cell probe station. The fuel was supplied from a gas cylinder of 5% H_2 balanced with Ar with ∼200 mL min⁻¹ flow rate, humidified via water bubbling at RT, and fed to the anode side. The current−voltage ($I-V$) characteristics were measured applying d.c. voltage bias between a contact of a Pt-coated tip on the cathodes exposed to laboratory air and the grounded anodes at elevated temperatures with 5 °C min⁻¹ ramping rate up to ∼510 °C in the use of software-controlled Keithley 2400 sourcemeter. After testing fuel cells, the morphology of Pt electrodes was observed using Carl Zeiss Ultraplus FESEM. A schematic diagram of μ-SOFC device under operation is illustrated in the cress-section view in Fig. 1. The device fabrication procedure and fuel cell measurement set-up are discussed in detail elsewhere [16,17]. To confirm pinhole-driven current leakage across electrolytes, ZrO_2 membrane resistance was estimated by $I-V$ characterization under d.c. voltage bias on μ-SOFC devices similar to those used for fuel cell tests at varying temperatures without fuel supply. EIS was carried out on selected μ-SOFC devices to estimate conductivity of ZrO_2 membranes at ∼510 °C applying a.c. voltage in the frequency range from ∼0.2 Hz to ∼1 MHz keeping both anodes and cathodes in air.

3. Results and discussion

3.1. Structural characteristics

As summarized in Fig. 2, glancing incidence XRD scans were conducted on as-grown and annealed ZrO_2 films on amorphous Si_3N_4-coated Si substrates of two different film thicknesses, ∼8 nm and ∼50 nm, to investigate the phase and grain growth behavior.

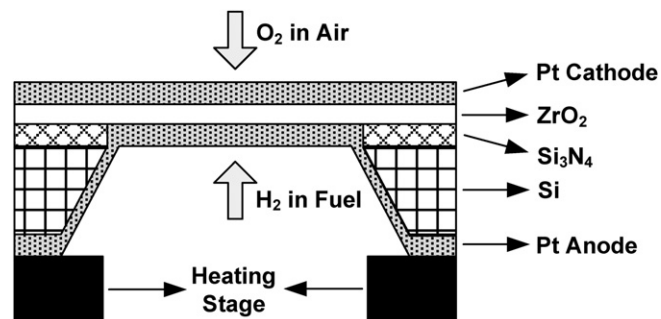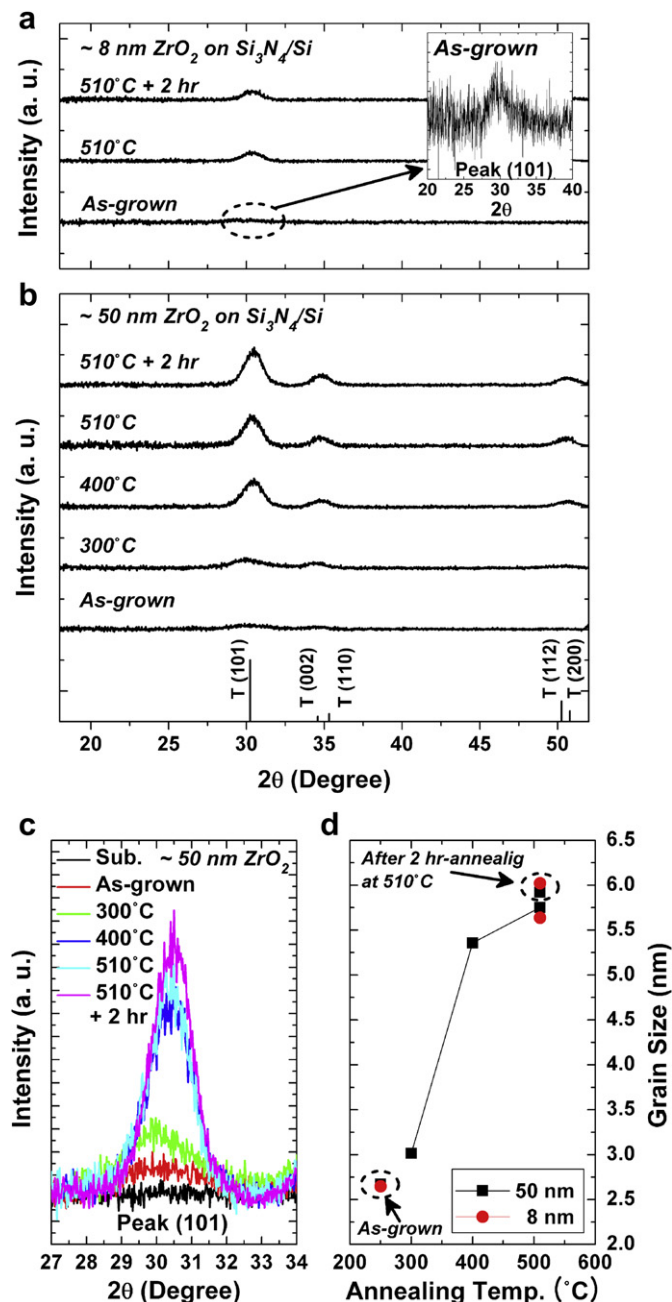**Fig. 1.** Cross-sectional schematic of a μ-SOFC. Pt anode covering the whole bottom of μ-SOFC device is electrically connected to heating stage.

Fig. 2. X-ray diffraction (XRD) profiles of two sets of as-grown and annealed ZrO_2 films of thickness (a) ~ 8 nm and (b) ~ 50 nm grown on Si_3N_4-coated Si substrates. The inset in (a) shows the magnified view of the (101) tetragonal ZrO_2 peak obtained from the as-grown ZrO_2 film. The reference XRD peaks of tetragonal ZrO_2 are shown at the bottom of (b) (ICDD-JCPDS Card No. 01-080-0965). (c) Detailed XRD scan results near the (101) tetragonal phase peak measured from ~ 50 nm-thick ZrO_2 films as-grown and annealed at varying temperatures from 300 °C to 510 °C. (d) Grain size vs. annealing temperature of ~ 8 and ~ 50 nm-thick ZrO_2 films including grain size measured as-grown and after annealing at 510 °C for 2 h.

Fig. 2(a) and (b) shows that ZrO_2 films oxidized even at RT are polycrystalline indicating the enhanced oxidation kinetics by photo-excitation. As the samples are heated to operating temperatures, their crystallinity is enhanced as can be seen in Fig. 2(c) and the tetragonal ZrO_2 phase is observed (ICDD-JCPDS Card No. 01-080-0965). While in the ZrO_2 bulk form, the tetragonal phase is known to be stable above ~ 1100 °C, nanometric ZrO_2 (crystallite size $< \sim 30$ nm) shows tetragonal structure likely due to the lower

surface energy of tetragonal phase than that of monoclinic phase consistent with previous studies [18–20]. The XRD peak narrowing is also observed upon heating and this generally indicates increase in grain size while there may be some contribution from strain relaxation due to annihilation of ionic defects such as oxygen vacancies by annealing. The approximate grain size was calculated from full width at half maximum of XRD peaks using Scherrer's formula and the results are summarized in Fig. 2(d). Grain growth becomes noticeable at around 300 °C and stabilizes above 400 °C. Upon 2 h annealing at 510 °C, only slight increase in grain size up to ~ 6 nm is observed regardless of film thickness. The estimated crystallite size is below the reported limit for stabilizing tetragonal phase and it can be expected that the majority portion of ZrO_2 membranes is in tetragonal phase during fuel cell operating conditions [21].

3.2. Mechanical stability of free-standing membranes

Before testing μ-SOFCs, the thermo-mechanical reliability of self-supported ZrO_2 membranes was evaluated by observing buckling patterns created after removing Si_3N_4 underlayers. Fig. 3 displays a series of optical microscopy images of representative ZrO_2 membranes of various thicknesses in the range from ~ 20 to 108 nm, which are clamped at the edges of the 160×160 μm^2 square windows of patterned substrate. Except for the ~ 20 nm-thick ZrO_2 membranes, four-fold rotational symmetry buckling patterns are observed similar to previous studies on YSZ-based membranes [6,17,22–24]. These characteristic buckling indicates that the membrane deformation is induced by residual compressive stress which might be formed through the volume expansion during oxidation of metal Zr to tetragonal ZrO_2 [24,25]. The buckling behavior is governed by the normalized pre-strain defined as $\langle \varepsilon_0 \rangle = \varepsilon_0 a^2/h^2$ where ε_0 is the physical pre-strain and a and h are the width and thickness of membrane respectively [23,25]. Accordingly, as evident in Fig. 3, with decreasing h keeping a constant, the membrane is buckled more since $\langle \varepsilon_0 \rangle$ increases in the negative direction (i.e. a/h ratio becomes larger). However, when membranes are thinner than critical thickness (~ 20 nm), buckling disappears representing that ε_0 also depends on membrane thickness. At very low thickness, pre-strain is slightly compressive or tensile and hence the membrane is flat with the full square symmetry preserved [25]. It is worth noting that regardless of buckling states, the majority of ZrO_2-based membranes are stable under the heating cycle during fuel cell measurements as well as high temperature annealing up to 600 °C verifying robust thermo-mechanical stability of free-standing pure ZrO_2 thin films [23].

3.3. Fuel cell experiments

To study the effect of electrolyte thickness on fuel cell performance, a set of μ-SOFCs were fabricated with ZrO_2 thin films of varying thickness from ~ 8 to 70 nm sandwiched with Pt electrodes deposited under identical conditions. As described earlier in Section 2.2, the μ-SOFC chips were measured while increasing temperature up to ~ 510 °C and supplying fuel and laboratory air to the anode and cathode respectively. Fig. 4(a) and (b) displays post fuel cell test FESEM images taken from the cathode and anode sides of the μ-SOFC with ~ 50 nm-thick ZrO_2 electrolytes respectively. The electrode surface morphology indicates that metal clusters underwent coarsening and agglomeration forming pores and electrical connection channels.

Fig. 5 shows the representative I−V characteristics and power density curves measured from μ-SOFC based on ~ 50 nm-thick ZrO_2 electrolyte with the peak power density, P_{peak}, of ~ 33 m W cm^{-2}, and OCV of ~ 0.91 V at 450 °C. Fig. 6(a) and (b) presents OCV and
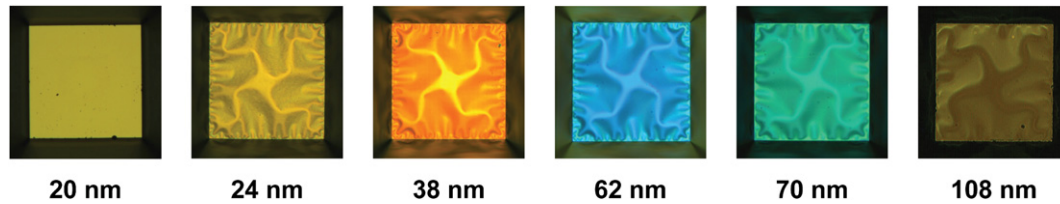
| 20 nm | 24 nm | 38 nm | 62 nm | 70 nm | 108 nm |

Fig. 3. Optical images of self-supported 160×160 μm^2 ZrO_2 membranes with varying thicknesses after Pt cathode deposition and reactive ion etching of Si_3N_4 layer.

P_{peak} data obtained from a set of representative ZrO_2 membranes of various thicknesses with increasing temperature. As shown in Fig. 6(a), the μ-SOFCs with electrolytes thicker than 30 nm show OCVs close to thermodynamic limit in the overall temperature range for fuel cell test (350–510 °C) similarly observed in YSZ-based μ-SOFCs [6]. This stability verifies that ZrO_2 films are high-quality dense films. However, notice that OCV abruptly drops when ZrO_2 membranes thickness is lower than ∼30 nm. The origin of this deviation of OCV from the theoretical value at low electrolyte thickness will be discussed later. As shown in Fig. 6(b), the fuel cell performance in terms of P_{peak} is more sensitive to ZrO_2 membrane thickness than OCV representing that the electrolyte thickness should be carefully optimized to compromise between leakage and oxygen-ion transport.

Also, in Fig. 6(b), one observes P_{peak} varies at elevated temperatures in a complex manner likely due to the combined effects of ionic conduction, decrease in microstructural defects, and the ripening of Pt electrode morphology under temperature ramping [16,22]. It is known that metal clusters undergo coarsening and agglomeration with temperature rise during fuel cell operation and the functional properties of μ-SOFCs are likely to be affected in the following scenario: (1) electrical paths are formed among metal particles that were originally isolated from one another and triple phase boundary (TPB) is activated leading to the initial abrupt increase in OCV above 200 °C (not shown here), (2) P_{peak} increases gradually with stable OCV and decreasing Ohmic loss across electrolytes at elevated temperatures, and (3) further agglomeration leads to the decrease in the total length of TPB degrading the fuel cell performance.

To verify the cause of significant ZrO_2 thickness effect on OCV particularly below ∼30 nm, leakage current measurements were conducted on membranes of various thicknesses in air. By fitting linear $I-V$ characteristics curves, the resistance of ZrO_2 membranes were calculated. Fig. 7 shows that the resistance and OCV measured at ∼510 °C show similar trends as a function of ZrO_2 thickness. While membranes are stably resistive at ∼70 nm, resistance drops abruptly with decreasing thickness at around ∼30 nm and below ∼20 nm, membranes are very leaky showing significant deviation from the predicted resistance given by scaling the resistance of ∼70 nm-thick membranes with thickness. The large standard deviation of measured resistances are given in the thickness range between ∼30 nm and ∼40 nm indicating that both electrically stable and leaky membranes exist in the same chip likely depending on exact materials synthesis conditions. Therefore, highly reliable fabrication process is required to achieve high fuel cell performance below ∼40 nm. The leaky devices show metallic characteristics with positive temperature coefficient of resistance corroborating that the low OCV is likely to be originated from the initial OCV drop by current leakage through pinhole-type microstructural defects in membranes that may be filled by Pt during fabrication process and form electrical short circuit channels between anodes and cathodes [17,26].

Fig. 8(a) and (b) shows the representative Nyquist plot measured on ∼70 nm-thick ZrO_2 electrolyte-based μ-SOFCs at ∼510 °C in air by EIS to estimate conductivity of nanostructured
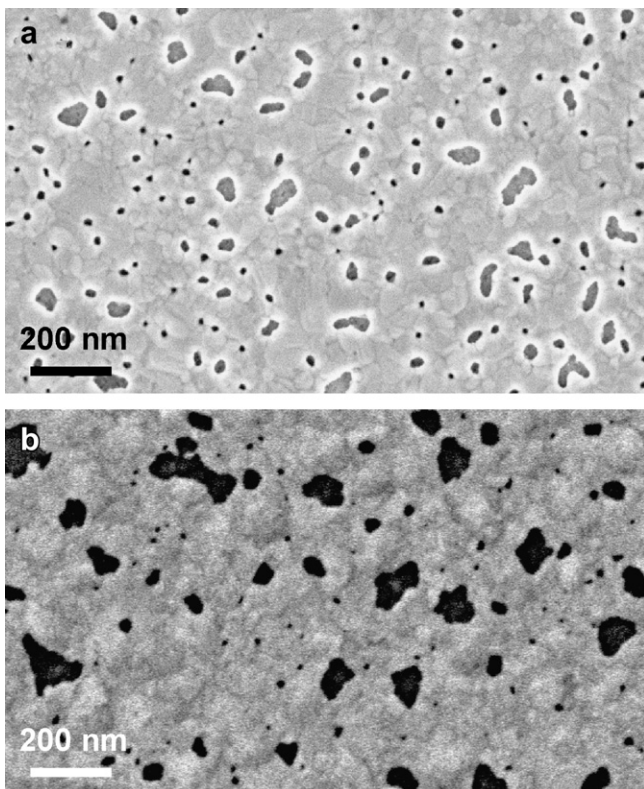

Fig. 4. Representative scanning electron microscope images of the surface morphology of (a) porous Pt cathode and (b) anode after fuel cell test.
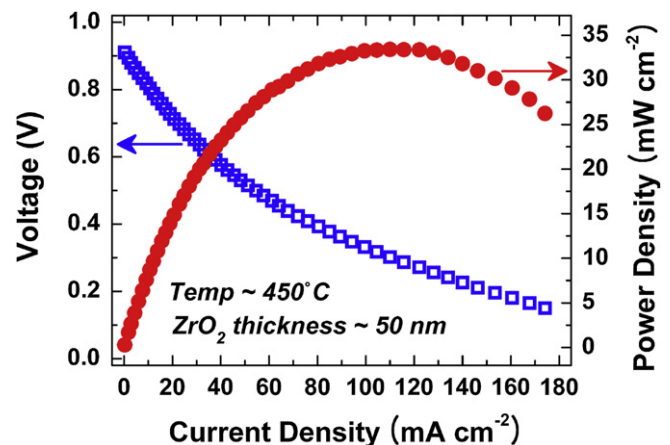

Fig. 5. Representative current/voltage sweep plot and power density curve measured from a μ-SOFC membrane of ∼50 nm-thick ZrO_2 electrolyte film at ∼450 °C during fuel cell operation. The maximum power density and open circuit voltage are estimated to be ∼33 mW cm^{-2} and ∼0.91 V respectively.
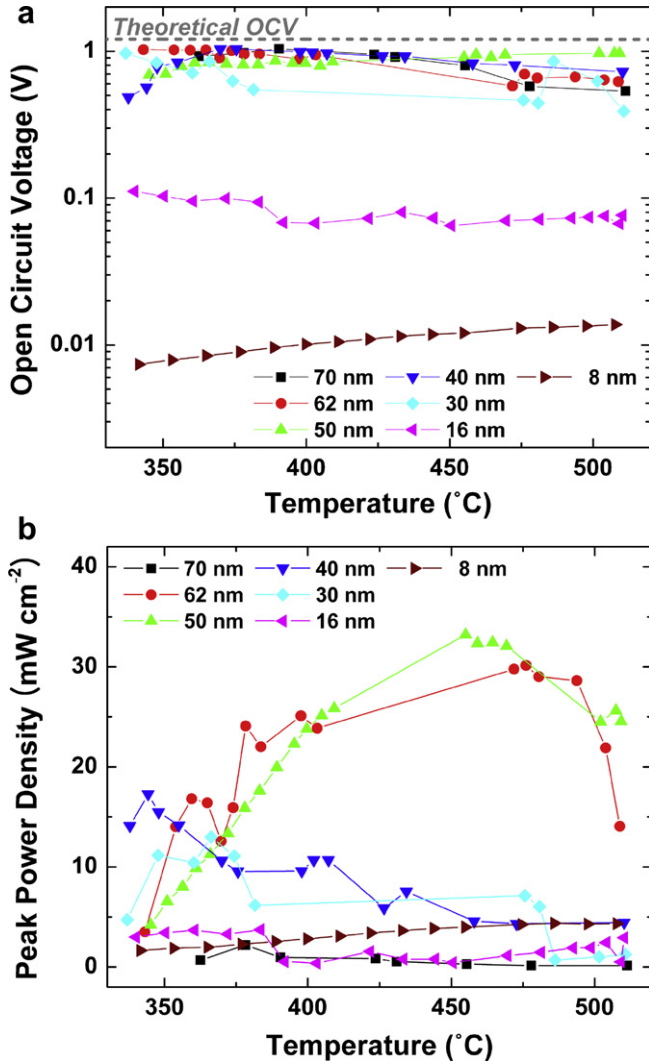
Fig. 6. Temperature dependence of (a) open circuit voltage (OCV) and (b) peak power density measured from μ-SOFC devices with ZrO_2 electrolytes of various thicknesses during temperature ramping for fuel cell operation.
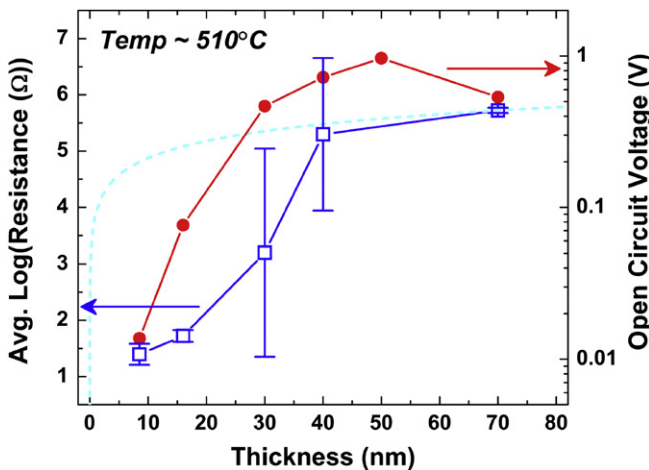

Fig. 7. Average resistance estimated from ZrO_2 membranes of varying thicknesses in μ-SOFC devices at ~510 °C in air without fuel supply along with OCV values measured under fuel cell operation at the same temperature taken from Fig. 6(b). The error bars and dashed line indicate the standard deviation of measured resistance values and the scaling of resistance with membrane thickness from the average resistance of ~70 nm-thick ZrO_2 electrolytes respectively.
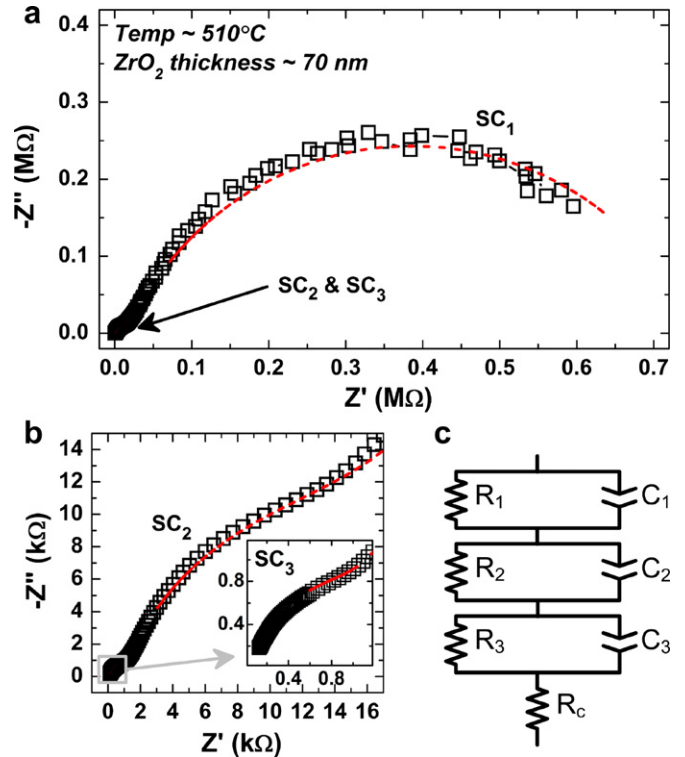

Fig. 8. (a) Nyquist plot obtained from AC impedance spectroscopy on ~70 nm-thick ZrO_2 membranes in μ-SOFC devices at ~510 °C in air. (b) The magnified Nyquist plot in high frequency regime. (c) Equivalent circuit model employed for fitting Nyquist plot. R_n and C_n represent resistance and constant phase element of semicircle SC_n respectively and R_c indicates a contact resistance element.

un-doped ZrO_2 layers. Three slightly overlapping semicircles are observed representing that three sets of reactions are activated with three distinguishable time scales as similarly observed in Pt/YSZ/Pt μ-SOFC structures by Holme et al. [27] The semicircle SC_3 observed in high frequency regime (675 kHz–1 MHz) is likely to be from the resistance of ZrO_2 electrolyte, while two other semicircles, SC_1 and SC_2, are found in the low (0.2 Hz–500 Hz) and intermediate frequency regimes (500 Hz–675 kHz) respectively and probably related to the electrode reactions [27].

Each semicircle SC_n is slightly depressed and hence, for equivalent circuit model analysis, can be expressed with combination of resistance and constant phase element (CPE) that are denoted by R_n and C_n respectively. Fig. 8(c) displays the equivalent circuit model for fitting Nyquist plot in whole frequency range which is composed of three RC circuits and one contact resistance element, R_c. The least squares fitting result is shown in Fig. 8(a) and (b) with dashed curves and the extracted R_3 value can be converted to the conductivity of ZrO_2 membranes. At ~510 °C, the conductivity is estimated to be ~3×10^{-5} S cm^{-1}. This value is higher than that of un-doped monoclinic ZrO_2 bulk but lower than those of polycrystalline YSZ bulk and nanometric YSZ thin films [9,28]. This intermediate conductivity value is probably due to fast ionic diffusion along grain boundaries in nanostructured ZrO_2 and enables μ-SOFC based on such membranes to be operable in the temperature range studied here [10].

3.4. Annealing effects

To investigate the range of functional properties of μ-SOFC using pure ZrO_2 electrolytes by post-deposition annealing on the electrolytes, we have compared the fuel cell performance of as-grown
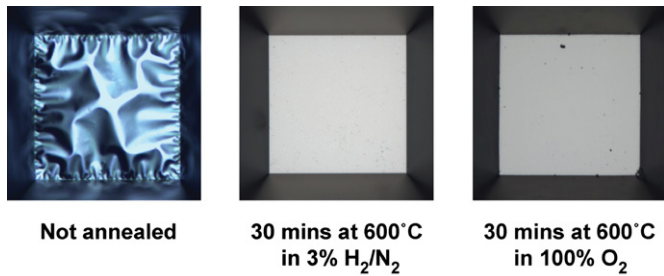
Fig. 9. Optical micrograph images of fully fabricated 160 × 160 μm² free-standing μ-SOFCs based on ∼50 nm-thick ZrO₂ membranes (a) as-grown and annealed at 600 °C for 30 min in (b) 3% H₂/N₂ and (c) 100% O₂.

and annealed membrane sets of three representative thicknesses: ∼ 8 nm, ∼30 nm, and ∼50 nm. Each set is composed of three μ-SOFC chips based on ZrO₂ electrolytes as-deposited and heat-treated at 600 °C in 3% H₂/N₂ and 100% O₂ for 30 min and prepared together through whole fabrication steps except the annealing process. The membranes were annealed before being coated with porous Pt electrodes and released from Si₃N₄ under-layers. Fig. 9 presents the optical microscope images of a set of fully fabricated μ-SOFC structures of ∼50 nm-thick ZrO₂ electrolytes as-grown and annealed in the reducing and oxidizing environments. While ∼8 nm-thick membranes are flat before and after annealing, the buckling patterns of ∼30 nm- and ∼50 nm-thick ZrO₂ elec-trolytes disappears by heat treatment indicating that the transition

occurs from compressive to tensile stress probably attributed to grain growth and coalescence, or diffusive relief of atomic peening similarly observed in other oxide systems such as YSZ and LSCF membranes [17,29]. Good thermo-mechanical stability of ZrO₂ membranes is maintained during fuel cell measurements.

Fig. 10(a) and (b) shows the effects of annealing on the func-tional properties of μ-SOFCs in terms of the maximum OCV and P_{peak} respectively. As shown in Fig. 10(a), the variations in OCV are less than 10% in μ-SOFCs of ∼30 nm- and ∼50 nm-thick electro-lytes. In ∼8 nm-thick ZrO₂-based μ-SOFC, although the OCV values are low, OCV is observed to be enhanced by over one order in magnitude upon O₂ annealing probably due to passivation of defects [6]. Kanashima et al. showed that the electronic leakage current was reduced by post-deposition annealing in O₂ at 600 °C by more than three orders of magnitude in ∼10 nm-thick ZrO₂ thin films [30]. The annealing in reduced environment also leads to increase in OCV in the thinnest membrane, but is less effective indicating there may be a contribution from near-surface oxygen stoichiometry on the OCV change. Fig. 10 (b) shows that the annealing effects on P_{peak} are evident up to electrolyte thickness of ∼30 nm. This may be related with defect healing as well as oxygen stoichiometry alteration in the ultra-thin oxide films under heating. In μ-SOFCs with ∼30 nm-thick electrolytes, while P_{peak} is increased by heat treatment in the reduced environment, the annealing in oxidizing ambient brings about a decrease. These results suggest that the ionic conduction in ZrO₂ electrolytes is tunable by modu-lating oxygen defects via annealing. However, in the case of μ-SOFCs based on ∼8 nm-thick electrolytes, regardless of anneal-ing environment, P_{peak} is observed to increase by three to four times indicating that the dominant contribution might be healing of microstructural defects as well as improvement in OCV.
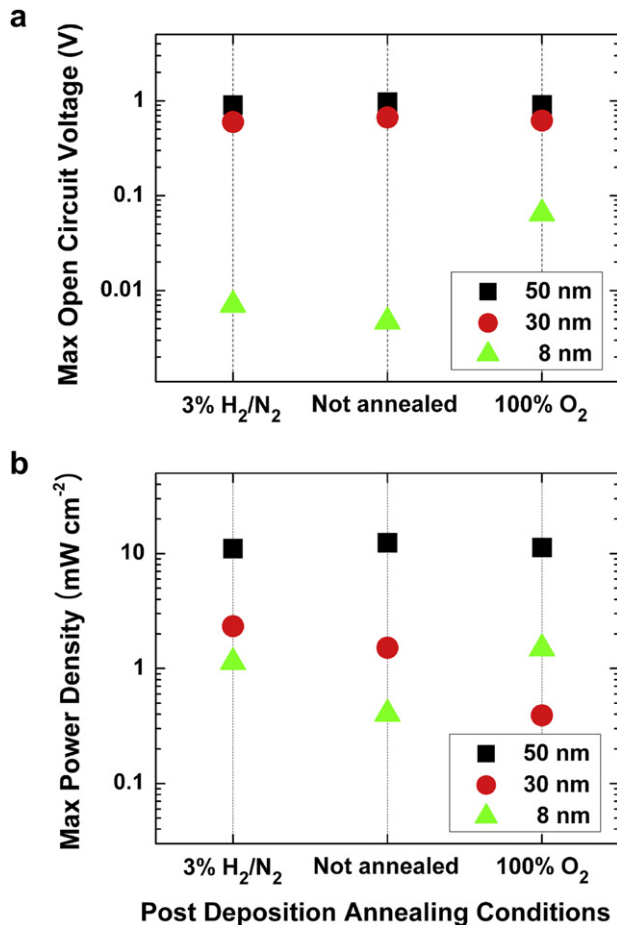
4. Conclusions

We have fabricated thin film SOFCs using self-supported membranes based on nanostructured un-doped ZrO₂ electrolytes and porous Pt electrodes. The fuel cells showed a peak power density of ∼33 mW cm⁻² with OCV of ∼0.91 V at 450 °C and thermo-mechanical stability. Oxygen annealing of ultra-thin elec-trolytes enhanced the OCV by nearly an order of magnitude and the peak power density by a factor of four. The dependence of func-tional characteristics of the micro-SOFCs on ZrO₂ electrolyte thickness has been studied in the sub-100 nm range.

Acknowledgments

Fig. 10. Comparison of (a) open circuit voltage and (b) maximum peak power density measured on μ-SOFC devices based on as-grown and annealed ZrO₂ electrolytes of three different thicknesses: ∼8 nm, ∼30 nm and ∼50 nm.

References

[1] S. Park, J.M. Vohs, R.J. Gorte, Nature 404 (2000) 265–267.
[2] S.J. Litzelman, J.L. Hertz, W. Jung, H.L. Tuller, Fuel Cells 8 (2008) 294–302.
[3] A. Evans, A. Bieberle-Hütter, J.L.M. Rupp, L.J. Gauckler, J. Power Sources 194 (2009) 119–129.
[4] E.D. Wachsman, K.T. Lee, Science 334 (2011) 935–939.
[5] H. Huang, M. Nakamura, P. Su, R. Fasching, Y. Saito, F.B. Prinz, J. Electrochem. Soc. 154 (2007) B20–B24.
[6] K. Kerman, B.-K. Lai, S. Ramanathan, J. Power Sources 196 (2011) 2608–2614.
[7] T.H. Etsell, S.N. Flengas, Chem. Rev. 70 (1970) 339–376.
[8] S.P.S. Badwal, Solid State Ionics 52 (1992) 23–32.
[9] W. Jung, J.L. Hertz, H.L. Tuller, Acta Mater. 57 (2009) 1399–1404.
[10] U. Brossmann, R. Wurschum, U. Sodervall, H.-E. Schaefer, J. Appl. Phys. 85 (1999) 7646–7654.

[11] D. Eder, R. Kramer, Phys. Chem. Chem. Phys. 8 (2006) 4476–4483.
[12] R.P. O'Hayre, S.-W. Cha, W. Colella, F.B. Prinz, Fuel Cell Fundamentals, John Wiley & Sons, Hoboken, New Jersey, 2006.
[13] G.D. Wilk, B. Brar, IEEE Electron Dev. Lett. 20 (1999) 132–134.
[14] S. Ramanathan, G.D. Wilk, D.A. Muller, C.-M. Park, P.C. McIntyre, Appl. Phys. Lett. 79 (2001) 2621–2623.
[15] C.-L. Chang, S. Ramanathan, J. Electrochem. Soc. 154 (2007) G160–G164.
[16] A.C. Johnson, B.-K. Lai, H. Xiong, S. Ramanathan, J. Power Sources 186 (2009) 252–260.
[17] B.-K. Lai, K. Kerman, S. Ramanathan, J. Power Sources 195 (2010) 5185–5196.
[18] R.C. Garvie, J. Phys. Chem. 69 (1965) 1238–1243.
[19] E. Djurado, P. Bouvier, G. Lucazeau, J. Solid State Chem. 149 (2000) 399–407.
[20] G. Baldinozzi, D. Simeone, D. Gosset, M. Dutheil, Phys. Rev. Lett. 90 (2003) 216103.
[21] S.C. Moulzolf, R.J. Lad, J. Mater. Res. 15 (2000) 369–376.
[22] K. Kerman, B.-K. Lai, S. Ramanathan, J. Power Sources (2012).
[23] C.D. Baertsch, K.F. Jensen, J.L. Hertz, H.L. Tuller, S.T. Vengallatore, S.M. Spearing, M.A. Schmidt, J. Mater. Res. 19 (2004) 2604–2615.
[24] N. Yamamoto, D.J. Quinn, N. Wicks, J.L. Hertz, J. Cui, H.L. Tuller, B.L. Wardle, J. Micromechan. Microeng. 20 (2010) 035027.
[25] V. Ziebart, O. Paul, H. Baltes, J. Microelectromech. Syst. 8 (1999) 423–432.
[26] A.C. Johnson, A. Baclig, D.V. Harburg, B.-K. Lai, S. Ramanathan, J. Power Sources 195 (2010) 1149–1155.
[27] T.P. Holme, R. Pornprasertsuk, F.B. Prinz, J. Electrochem. Soc. 157 (2010) B64–B70.
[28] M.M. Nasrallah, D.L. Douglass, J. Electrochem. Soc. 121 (1974) 255–262.
[29] D.J. Quinn, B. Wardle, S.M. Spearing, J. Mater. Res. 23 (2008) 609–618.
[30] T. Kanashima, S. Kaitai, M. Sohgawa, H. Kanda, M. Okuyama, Proceedings of the 13th IEEE Int. Symp. Appl. Ferroelectrics (2002) pp. 199–202.